Journal of Physics: Conference Series **758** (2016) 012003 doi:10.1088/1742-6596/758/1/012003

$NaTaO_3$/MCM-48 composites for photocatalytic conversion of organic molecules

K Senevirathne,[1,2,6] **C-K Xia**,[1,7] **S P Adhikari**,[1,5] **L Zhang**,[3] **R T Williams**,[1,4] **and A Lachgar**[1,5,8]

[1]Center for Energy, Environment, and Sustainability, Wake Forest University, Winston-Salem, NC 27109 USA
[2]Department of Chemistry, Florida A & M University, Tallahassee, FL 32307
[3]Joint School of Nanoscience and Nanoengineering, North Carolina Agricultural and Technical State University and the University of North Carolina at Greensboro, Greensboro, NC 27401
[4]Department of Physics, Wake Forest University, Winston-Salem, NC 27109
[5]Department of Chemistry, Wake Forest University, Winston-Salem, NC 27109

Abstract

The synthesis, characterization, and photocatalytic activity of a series of $NaTaO_3$/MCM-48 composite photocatalysts prepared by sol-gel method is reported. The composite catalysts were investigated by powder X-ray diffraction (XRD), scanning electron microscopy (SEM), and N_2 adsorption-desorption porosimetry. Their photocatalytic activity for conversion of organic molecules was tested using *p*-nitroaniline as a model pollutant. The surface area was found to be in the order of 235-964 m^2/g and 35-407 m^2/g for photocatalysts calcined at 500 °C and 850 °C, respectively. The surface area was found to depend on the MCM silica content. The pore size for samples calcined at 500 °C ranges from 2.6-3.2 nm, and becomes significantly larger at 850 °C (12.6-30.0 nm) for most composites. All composites have been found to be photocatalytically active towards *p*-nitroaniline conversion into *p*-phenylenediamine under uv-visible irradiation. The conversion of *p*-nitroaniline per weight of $NaTaO_3$ in the composite photocatalysts is found to be higher than that of pristine $NaTaO_3$. The composites lose 12% of their original activity after three consecutive catalytic cycles.

Keywords: Composites, photocatalysts, sodium tantalate, *p*-nitroaniline conversion

[6] Corresponding authors:
Keerthi Senevirathne
E-mail:keerthi.senevirathne@famu.edu
Department of Chemistry, 1530, S. martin Luther King Jr. Blvd, Tallahassee, FL 32307

[7] Current affiliation: School of Chemistry and Chemical Engineering, Jiangsu University, Zhenjiang, 212013, China

[8] Abdou Lachgar
Email: lachgar@wfu.edu
Department of Chemistry, Salem Hall, P.O. Box 7486, Winston-Salem, NC 27109-7486

1. Introduction

Many efforts have been devoted to developing heterogeneous photocatalysts to harness solar energy for hydrogen generation, pollution remediation, and organic molecule conversion[1] . Among the large number of photocatalysts, $NaTaO_3$ with perovskite-type structure was prepared using a wide range of synthetic methods such as solid state reactions[2], hydrothermal synthesis[3], and template-assisted sol-gel synthesis[4], and was extensively studied in photochemical[5, 6] or photoelectrochemical[7, 8] hydrogen generation via water splitting. In addition, there are a few reports in the literature that discuss its application in pollution remediation[9-11]. Yokoi and co-workers have applied a confined space synthesis method to make nanoparticulate $NaTaO_3$ and explore the effect of photocatalysts' morphology on its activity, and found nanostructured $NaTaO_3$ was three times as active as $NaTaO_3$ prepared by high temperature solid state reactions[4]. Perovskite type $NaTaO_3$ is a catalyst with significant water splitting ability under uv irradiation because of its bandgap energy and band structure. Bandgap energy calculated for $NaTaO_3$ by applying Kubelka-Munk method to diffuse reflectance data is 4.0 eV[12]. The band structure of $NaTaO_3$ is positioned in such a way that it can catalyze both oxidation and reduction reactions in water splitting[13]. Kato and co-workers studied Lanthanum (La^{3+}) doped $NaTaO_3$ and observed the highest quantum yield ever reported– (56%)- under UV irradiation at 270 nm[14]. Li and co-workers used the same material in order to evaluate the structural and optical effects of La^{3+} doping and evaluated its photocatalytic activity using decomposition of a model dye, Safranine T[10]. They attributed the enhanced photocatalytic activity to easy excitation of electrons from the valence band to the conduction band due to La^{3+} doping, in contrast to Kudo's conclusion that smaller particle size and ordered surface nanostep structure is responsible for the observed enhanced activity. Yi and co-workers utilized 1-D nanofibers of $NaTaO_3$ prepared by electrospining to evaluate photodegradation of methylene blue and concluded that the 1-D nature of the photocatalyst effectively enhances the photodecomposition of dye molecules[11]. Mohamed and co-workers reported the synthesis of Pd decorated $NaTaO_3$ photocatalyst and its use in environmental remediation of aqueous nitrate solutions, and observed that $Pd/NaTaO_3$ was photocatalytically active under visible light with $\lambda > 420$ nm even though its band gap data suggest a band edge at about 360 nm[15].

It is commonly acknowledged that high surface area benefits photocatalytic activity due to the availability of a larger number of active sites and enhanced substrate adsorption on the catalyst surface[16]. High crystallinity of the photocatalyst is also desired, since it minimizes photoexcited electron-hole pair recombination by decreasing the defects concentration. However, it is difficult to achieve both high surface area and crystallinity by regular synthesis methods because latter is achieved at higher temperatures, which generally leads to larger particle size, hence lower surface area. There are several advantages of using a mesoporous host material to support photocatalysts. High surface area, long range order, and uniform pore size allow uniform dispersion and prevent agglomeration of photocatalysts during high temperature synthesis and photocatalytic testing. In many instances, confinement of photocatalysts within the host pore structure tends to longer life time of the exciton, leading to enhanced catalytic activity[17]. MCM-48 (Mobile crystalline mesoporous) silica is highly ordered, high surface area silica template, which is a good candidate for catalytic applications due to its favorable mass transfer kinetics compared to other silica templates such as MCM-41[18]. Peng and co-workers studied the encapsulation of CdS visible light photocatalyst in MCM-48 and its photocatalytic activity towards water splitting, and found the composite to be highly active with 16.6% quantum yield[19].

Since surface area and catalyst distribution seem to be important factors that affect catalytic properties, we utilized a high surface area silica template (MCM-48) to homogenously disperse $NaTaO_3$ catalyst and form a composite. Specifically, $NaTaO_3$/MCM-48 composite photocatalysts were prepared by applying a sol-gel synthesis method and subsequent calcination in air. The effect of synthesis conditions on structural integrity, pore size distribution, and surface area of MCM-48 and $NaTaO_3$/MCM-48 composite catalysts were investigated by applying a wide range of analytical techniques including Powder X-ray diffraction (PXRD), BET surface area, thermogravimetric analysis

(TGA), and electron microscopy (EM). The photocatalytic activity of $NaTaO_3$/MCM-48 composite catalysts was subsequently evaluated using *p*-nitroaniline (*p*-NA) conversion into *p*-phenylenediamine (*p*-PDA) as a model reaction. The *p*-PDA is an important component in many industrial chemicals such as rubber antioxidants, thermoplastics, and textile fibers[20]. Developing a facile and economic route to synthesize *p*-PDA would be of interest due to rigorous synthetic conditions required in most commonly used commercial hydrogenation methods.

2. Experimental

2.1. Materials

Sodium acetate (NaAc, Aldrich), tantalum chloride ($TaCl_5$, Aldrich), citric acid (Fisher Scientific), absolute ethanol (EtOH, 200 proof, Pharmco-AAPER), dihydrogenhexachloroplatinate hexahydrate (H_2PtCl_6-$6H_2O$, Aldrich), ethylene glycol, *p*-nitroaniline (4-$C_6N_2O_2H_6$, Aldrich), cetyltrimethylammonium bromide (CTAB, 98%, Alfa Aesar), and tetraethylorthosilicate (TEOS, 98%) were used without further purification. De-ionized water was used in all the preparations.

2.2 Materials Synthesis

*2.2.1. MCM-48***.** Mesoporous MCM-48 silica was synthesized following a procedure outlined in the literature[21]. Briefly, 1.2 g of surfactant CTAB was mixed with 50 mL of de-ionized water by vigorous stirring. Then, 25 mL of EtOH and 6 mL of 36% aq. ammonia were added to the surfactant solution and stirred for 10 minutes. Next, 1.8 mL (8 mmol) of TEOS was added and the mixture was stirred for 4 hours at room temperature to form a colorless precipitates, which was collected by centrifugation, washed 3 times with de-ionized water, and dried at 80 °C overnight. The product was ground, and then calcined at 550 °C for 6 hours in air with heating and cooling rates of 3 °C /min.

2.2.2. $NaTaO_3$. A literature reported sol-gel method was used for the synthesis of $NaTaO_3$ [22]. Sodium acetate (NaAc) and tantalum chloride were used as precursors, and citric acid (CA) was used as complexing agent. In a typical experiment, NaAc (0.23 g, 2.79 mmol) and CA (2.93 g, 14 mmol) were dissolved in a minimum amount of de-ionized water (~5 mL). The required amount of $TaCl_5$ (1.0 g, 2.79 mmol) was dissolved in 10 mL of EtOH. Then, NaAc-CA mixture was added dropwise to $TaCl_5$ solution and stirred for one hour. The mixture was heated in an oil bath at 80 °C until gelation occurred and a colorless precipitate was formed., The product was dried, then calcined at 350 °C for one hour and 500 °C for 3 hours in air at a heating and cooling rate of 3 °C / min to remove all organic components and to form $NaTaO_3$.

*2.2.3. $NaTaO_3$/MCM-48 composite synthesis***.** Required amounts of MCM-48 silica,NaAc, $TaCl_5$, and citric acid for the preparation of $NaTaO_3$ / MCM-48 composite were calculated using the MCM-48/$NaTaO_3$ mass ratio. Precursor solutions for $NaTaO_3$ were prepared as described in the $NaTaO_3$ synthesis section. The required amount of MCM-48 was placed in a beaker and the $NaTaO_3$ precursor solution was added dropwise. The mixture was stirred for 1 hour prior to heating at 80 °C in an oil bath until gelation and dry material was formed. The gel was calcined at 350 °C for 1 hour and then at 500 °C or 850 °C for 3 hours at a heating and cooling rate of 3 °C / min.

2.2.4. Pt deposition. 1 wt% of Pt used as co-catalyst was deposited on each catalyst by microwave-assisted polyol reduction method. 0.25 g of photocatalyst was mixed with 10 mL of ethylene glycol and sonicated for 1-2 hours in order to uniformly disperse the catalyst. Next, 0.007 g of Pt precursor ($H_2PtCl_6.6H_2O$) was dissolved in ~2 mL of ethylene glycol and mixed with dispersed photocatalyst by stirring overnight. Reduction of Pt precursor was carried out under microwave irradiation for 3 minutes at 180 ºC. The sample was recovered by centrifugation, and several washings with de-ionized water were performed to remove ethylene glycol. The sample was dried in an oven at 70 ºC overnight.

2.3 Physical Characterization

2.3.1. Powder X-ray diffraction (PXRD). A Bruker-AXS D2 Phaser powder X-ray diffractometer (PXRD) equipped with a Ni-filtered Cu K□ sealed X-ray tube (□=1.54184 Å) and a Lynxeye position-sensitive detector was used for X-ray analysis. The diffractometer was operated at 30 kV and 10 mA with a step width of 0.015° and a scan rate of 1.5°/min. PXRD data were collected at room temperature and analyzed using the Bruker-AXS EVA software package.

2.3.2. Scanning Electron Microscopy (SEM). A Carl Zeiss Auriga-BU FIB FESEM scanning electron microscope was employed to examine morphologies of all $NaTaO_3$/MCM-48 composite samples. A small amount of sample was spread on a carbon tape attached to an aluminum stub. The stubs were then mounted on a sample holder and examined.

2.3.3. Thermogravimetric analysis (TGA). A Perkin Elmer Pyris 1 thermogravimetric analyzer was used to determine thermal stability and crystallization temperature of $NaTaO_3$/MCM-48 composite. The composite was heated up to 1000 °C with a temperature ramp rate of 5°C min^{-1} in a continuous air flow.

2.3.4. Surface area and porosity analysis. A Quantachrome ASiQC 0100-2 Surface Area Analyzer was used in surface area and porosity analysis at 77 K. Microcrystalline samples were outgassed at 120 ºC for 2 hours prior to analysis. The samples' specific surface area and pore size distribution were evaluated using the Brunauer-Emmet-Teller (BET) method. The pore size distribution was analyzed using a function, which applies the Density Functional Theory (DFT) built into ASiQwin software.

2.3.5. Elemental analysis. Elemental analysis of synthesized catalysts was carried out using inductive coupled plasma (ICP) and atomic absorption spectrometric (AAS) analysis. A Prodigy High Dispersion ICP OES (Teledyne Leeman Labs, USA) instrument and a calibration curve method were used to quantify the amounts of Na, Ta, and Si in solid catalysts. The solids were dissolved in Conc. nitric acid in an acid digestion autoclave by heating at 200 ºC for 24 hours.

2.4 Photocatalytic experiments

Photocatalytic activity of the prepared compounds was evaluated using the following procedures. The photocatalytic reaction was carried out using an outer-irradiation reaction photo-cell connected to an inert gas line (argon). Photocatalyst powder (0.1 g) was dispersed in 30 mL of 20 ppm aqueous *p*-nitroaniline solution and stirred for ~30 min in an argon atmosphere, prior to irradiation. The suspension was then irradiated with a 200 W super-pressure mercury lamp (calculated power density, 10.2 W/cm^2) to initiate the conversion reaction. At a given irradiation time interval, a small aliquot (1.0 mL) was drawn from the system by a syringe, centrifuged to remove any advertently trapped catalyst, and analyzed with an Agilent 8453 UV-visible spectrophotometer. The conversion of *p*-nitroaniline was monitored by measuring the absorbance at λ_{max} = 238 and 380 nm, which corresponds to product and precursor peaks, respectively. Photocatalytic reproducibility tests were carried out as follows. After first catalytic testing, the solid catalyst was recovered by centrifugation and washed with de-ionized water in order to remove residual *p*-nitroaniline and/or *p*-phenylenediamine followed by drying in vacuum.

3. Results and Discussion

3.1. Structural analysis

The structure of mesoporous MCM-48 silica was confirmed by low angle PXRD. Figure 1 shows PXRD patterns of MCM-48 silica and $NaTaO_3$/MCM-48 composites calcined at 500 and 850 °C in air. The PXRD pattern of MCM-48 silica shows two significant peaks at 2θ = 2.7° and 3.2°, corresponding to (211) and (220) crystallographic planes, respectively. It is evident from Figure 1a that high calcination temperature of MCM-48 silica has an effect on intensity of the PXRD peaks; peak intensity

decreases with increasing calcination temperature due to a decrease in scattering contrast between pores and pore walls[21]. High temperature treatment by itself does not destroy the MCM-48 silica structure. However, the presence of the complexing agent (i.e. citric acid) coupled with high temperature calcination has a detrimental effect on the MCM-48 silica structure and causes the cubic structure to collapse. As shown in Figure 1b, the signature PXRD reflection that appears at $2\theta = 2.7°$ for MCM-48 silica is absent from MCM-48 silica treated with citric acid and high temperature. Similarly, incorporation of $NaTaO_3$ also causes changes in the silica MCM-48 structure.

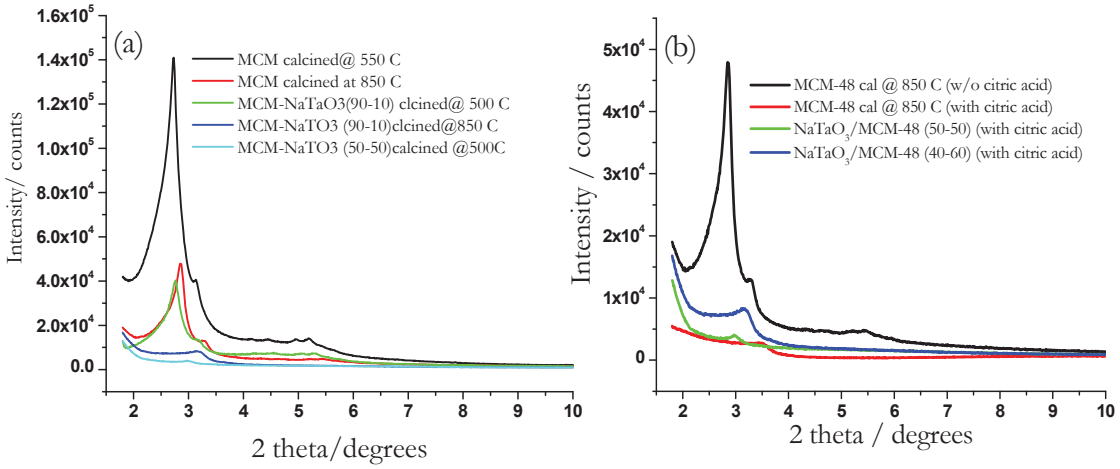

Figure 1. (a) Low angle X-ray diffraction patterns of silica MCM-48 and $NaTaO_3$-MCM composite catalysts calcined at different temperatures. (b) Figure shows XRD patterns of silica MCM-48 prepared in the presence and absence of citric acid along with composites calcined at 850 °C.

According to the literature and our experiments, $NaTaO_3$ prepared by sol-gel method and calcined at 500 °C is crystalline. Therefore, initially we used this temperature as the calcination temperature of composite catalysts. However, the composite catalysts prepared at this temperature were amorphous and no detectable XRD peaks were observed. Even though crystallinity is a highly important factor in photocatalysis, Tüysüz and co-workers reported photocatalytic water splitting using porous but amorphous $NaTaO_3$ and reported that better catalytic activity was observed for the amorphous over the crystalline phase[23]. In order to discern the calcination temperature that makes crystalline composite catalysts, thermogravimetric analysis (TGA) data was acquired (Figure 2). When $NaTaO_3$ was heated in air three prominent weight losses at 250-500 °C, 500 - 550°C, and 800 - 850 °C are observed (Figure 2a). The major weight loss between 250-500 °C may be attributed to loss of carbon, which is coming from the citric acid complexing agent. The second weight loss observed at 500 °C corresponds to calcination of $NaTaO_3$, as reported in the literature. This weight loss is not visible in the $NaTaO_3$/MCM composite catalyst (Figure 2b) which is consistent with PXRD data, which shows amorphous structure. After the third weight loss approximately at 850 °C, a stable phase was observed. Therefore, we selected 850 °C as the calcination temperature of composite catalysts based on the second calcination temperature, i.e. third weight loss, of $NaTaO_3$ (Figure 2a). It should be noted that the structure of MCM-48 slightly changes, according to XRD data (Figure 1a) and this might be the reason why we see a weight loss at 850 C for composites, but not pure $NaTaO_3$.

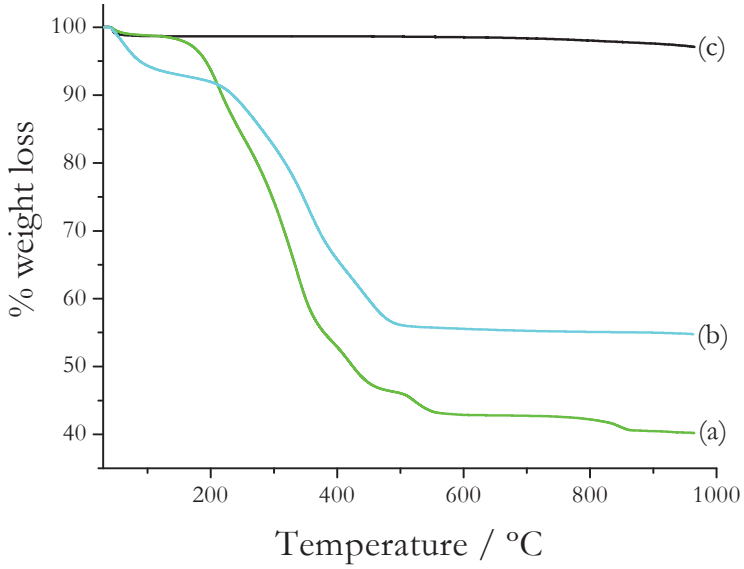

Figure 2. Thermogravimetric plots of (a) $NaTaO_3$, (b) $NaTaO_3$/MCM-48, (c) silica MCM-48 heated in air.

Powder X-ray diffraction was employed to evaluate the structure and crystallinity of $NaTaO_3$/MCM-48 composite catalysts. Figure 3 represents the PXRD plots of $NaTaO_3$/MCM-48 composites calcined at 850 °C for 3 hours in air along with $NaTaO_3$ calcined at 500 °C. The PXRD pattern of $NaTaO_3$/MCM-48 composites matches well, in terms of peak positions and intensity; with orthorhombic $NaTaO_3$ (PDF # 00-025-0863). Interestingly, composite catalysts calcined at 500 °C in air are amorphous (not shown) even though $NaTaO_3$ prepared without any silica MCM-48 is crystalline at that temperature. Since crystallinity is an important parameter in photocatalysts, higher temperature calcination is essential in order to form a crystalline phase of $NaTaO_3$. The crystallite size of $NaTaO_3$ in the composites calcined at 850 °C was calculated by applying the Debye-Scherer equation (Eqn. 1)[24].

$$B = \frac{0.9\,\lambda}{FWHM \times \cos\theta} \qquad \text{Eqn 1}$$

Where B is crystallite size, λ is the wavelength, FWHM is full width at half maximum of the peak at $2\theta = 46.59°$ chosen because background interference originating from silica is minimal above $2\theta = 40°$. The calculated crystallite size of pure $NaTaO_3$ calcined at 500 °C is approximately 23 nm while crystallite size of $NaTaO_3$ in $NaTaO_3$/MCM-48 composites ranges from 11 to 22 nm depending on $NaTaO_3$ content. The $NaTaO_3$/MCM-48 composites with 10% and 50% $NaTaO_3$ exhibited the smallest and largest $NaTaO_3$ crystallite size, respectively. Apparently, crystallite size of $NaTaO_3$ decreases with the increase of silica MCM-48 content.

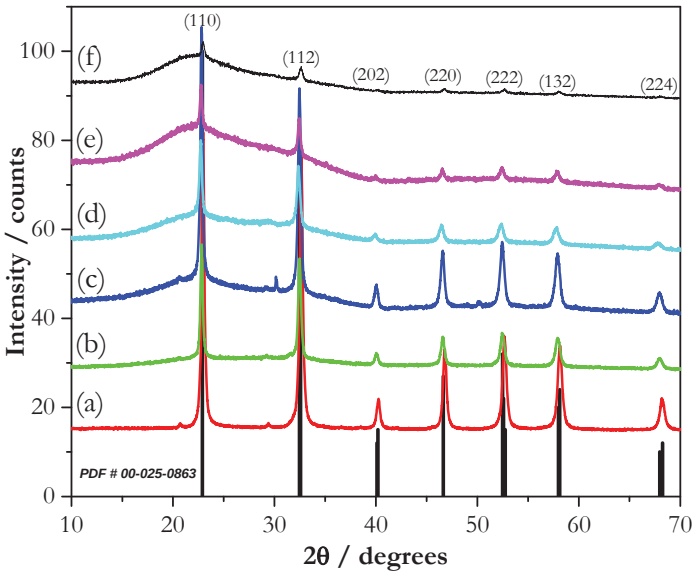

Figure 3. Powder X-ray diffraction patterns of $NaTaO_3$/MCM-48 composites calcined at 850 ºC for 3 hours in air. The $NaTaO_3$/MCM-48 ratio changes as (a) 100/0 calcined at 500 ºC, (b) 50/50, (c) 40/60, (d) 30/70, (e) 20/80, and (f) 10/90.

3.2. BET Surface area and pore size distribution analysis

Surface area and porosity of silica MCM-48, $NaTaO_3$, and $NaTaO_3$/MCM-48 composite materials were studied by nitrogen adsorption-desorption isotherms data. Figure 4 represents physisorption isotherms of silica MCM-48, $NaTaO_3$, and $NaTaO_3$/MCM-48 composites samples. Silica MCM-48 shows typical reversible type IV isotherm even though the hysteresis loop is not prominent and higher P/P_0 region is a spike instead of a plateau. However, the inflection point, which clearly distinguishes the transition from monolayer adsorption to multilayer adsorption, is prominent. Additionally, this marked inflection, which is caused by capillary condensation, is an indication of the mesoporous nature of silica MCM-48[21]. The sharpness of the inflection remained unchanged when MCM-48 silica was calcined at 850 °C (Figure 4e) indicating that highly ordered mesoporous structure of MCM-48 silica is not significantly altered even after calcination, which supports PXRD data. The surface area of MCM-48 synthesized in this work is in the range of literature reported values (1270 vs 1281 m^2/g)[18]. However, compared to MCM-48 calcined at 500 °C, the adsorption-desorption isotherms for MCM-48 calcined at 850 °C (Figure 4e and Table 1) showed lower N_2 adsorption and lower BET surface area,1270 vs. 1011 $m^2.g^{-1}$ (Figure 4f and Table 1)]. However, isotherms for $NaTaO_3$ and $NaTaO_3$/MCM-48 composites (Figure 4c-d) calcined at 850 °C show a plateau at lower P/P_0 region. This suggests that high temperature treatment diminishes the mesoporosity and attractive interactions between N_2 adsorbate and the $NaTaO_3$ surface are weaker than interactions among N_2 molecules.

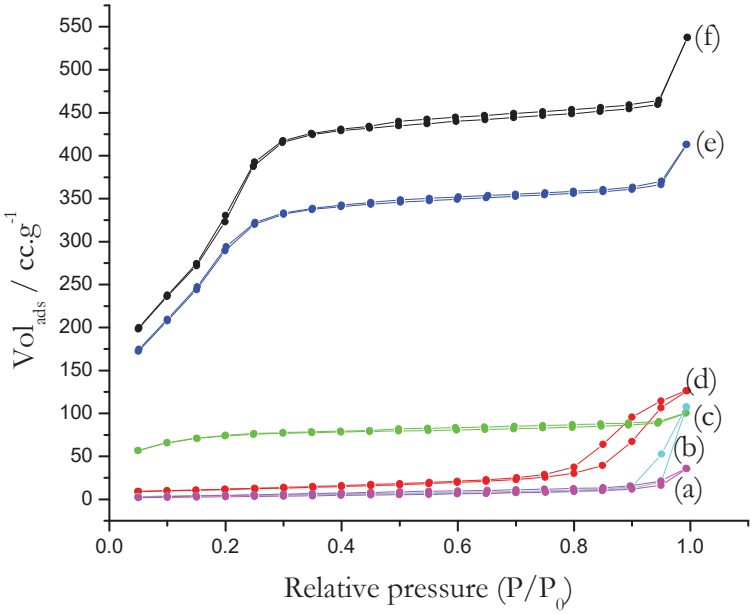

Figure 4. Nitrogen adsorption-desorption isotherms of $NaTaO_3$/MCM-48 (50/50 ratio) (a), $NaTaO_3$ (b), and silica MCM-48 (e) heated at 850 °C for 3 hours in air. (c), (d), and (f) represent $NaTaO_3$/MCM-48 (50/50 ratio), $NaTaO_3$, and silica MCM-48, respectively, calcined at 500 °C for 3 hours in air.

The BET surface area, pore size, and pore volume of composite photocatalysts are tabulated in Table 1. The average pore diameter and volume were calculated by applying a density functional theory (DFT) model, in which silica with cylindrical pores is considered to be the adsorbent, into adsorption branch. DFT model provides a more realistic pore size distribution, In this model, the local fluid structure near curved solid walls is clearly defined and pore distribution is determined by intermolecular potentials of the fluid-fluid and solid fluid interactions[25]. In contrast classical macroscopic theories such as Barrett- Joyner- Halenda (BJH) do not provide a realistic description of filling of micro and narrow mesopores and underestimate pore size distribution. In this method, pore size was found to be largely uniform for all samples calcined at 500 °C, in the range of 26-32 Å (Figure 5a). The average pore size of MCM-48 silica calcined at 500 °C is 32 Å and decreases to ~29 Å upon calcination at 850 °C, but it is still in the meso regime. In contrast, pure $NaTaO_3$ possesses relatively larger inter-grain mesopores (126-294 Å) after processing in the 500-850 °C temperature range. As shown in Table 1, the pore sizes of $NaTaO_3$/MCM-48 composite catalysts calcined at 500 °C are similar to that of silica MCM-48 except at higher $NaTaO_3$ loading (40-50 % loading). However, pore volume shows a systematic decrease upon increase in $NaTaO_3$ content (Figure 5a). Nevertheless the pore structure of all composite catalysts calcined at 850 °C, except those with $NaTaO_3$ loading 10 and 20%, have collapsed resulting in a relatively small pore volume.

Table 1. Surface area, pore diameter, and pore volume of $NaTaO_3$/MCM-48 composites.

Nominal $NaTaO_3$ /MCM-48 ratio	BET surface area / $m^2.g^{-1}$		Pore diameter (Å) (adsorption)		Pore volume / $cm^3.g^-$ (adsorption)	
	500 °C	850 °C	500 °C	850 °C	500 °C	850 °C
MCM	1270	1011	32	29	0.767	0.590
$NaTaO_3$	40	15	126	294	0.185	0.135
10/90	964	407	32	26	0.549	0.246
20/80	866	139	32	26	0.512	0.133
30/70	538	96	32	300	0.318	0.041
40/60	278	68	26	300	0.185	0.037
50/50	235	35	26	300	0.145	0.048

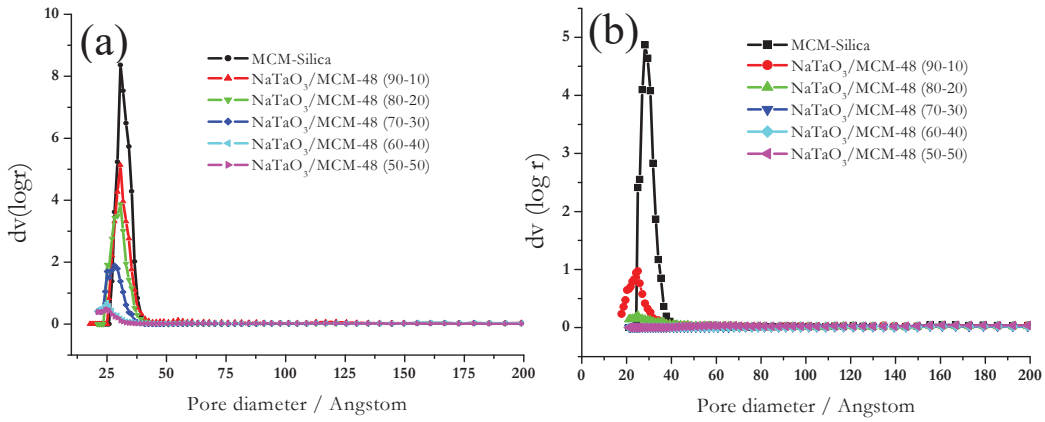

Figure 5. Pore size distribution of MCM-48 and composites calcined at (a) 500 °C and (b) 850 °C

3.3. Morphological characterization

SEM images of MCM-48 and $NaTaO_3$/MCM-48 composites are shown in Figure 6. MCM-48 calcined at 500 °C in air is spherical in shape and polydispersed. The particle size ranges from about 0.2 – 1 micron. Calcination of MCM-48 at 850 °C does not significantly change the morphology (Figure 6(b)). Similarly, the composite with 10% $NaTaO_3$ retains its spherical morphology. However, a significant change in morphology is evident in the composite with higher $NaTaO_3$ content (50%) (Figure 6(c)), which consists of a mixture of large particles and some spheres indicating 50% loading is too much. It is possible that excess $NaTaO_3$ catalyst crystallizes outside the MCM-48 pores.

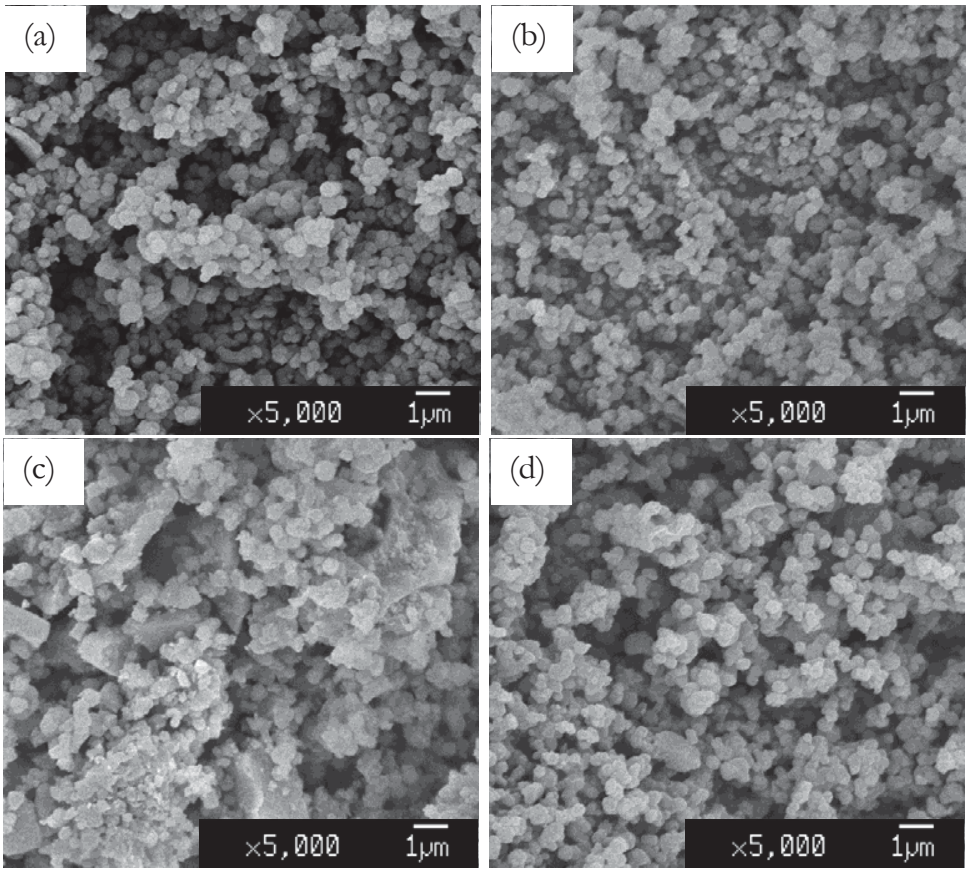

Figure 6. SEM images of MCM-48 calcined at 500 °C (a) and 850 °C (b). Figure (c) and (d) show 50-50 and 10-90 $NaTaO_3$/MCM-48 composites calcined at 850 °C.

3.4. Photocatalytic activity

Photocatalytic activity of the Pt/$NaTaO_3$/MCM-48 composite catalysts was evaluated by investigating the conversion of *p*-nitroaniline (*p*-NA) to *p*-phenylenediamine (*p*-PDA) under uv irradiation using a 20 ppm aqueous solution of *p*-nitroaniline. The experiments were carried out at room temperature with continuous argon purge at atmospheric pressure, in the absence of hole-scavengers. The conversion analysis of *p*-NA solution was made spectrophotometrically by assessing its decrease in absorbance at 380 nm. The Figure 7 shows the evolution of absorbance change of *p*-NA as a function of time during photocatalytic reduction. The photocatalytic activity, in terms of *p*-NA conversion was calculated using the decrease in absorbance at 380 nm. As shown in Figure 7a, relative change in the absorbance of *p*-NA in the absence of photocatalyst is negligible, which indicates that light irradiation alone has no effect on *p*-NA conversion. In the presence of photocatalysts, a significant decrease of the absorbance at 380 nm along with simultaneous appearance of an absorption band at 238 nm, the characteristic absorbance peak of *p*-PDA, was observed (Figure 7b-d).

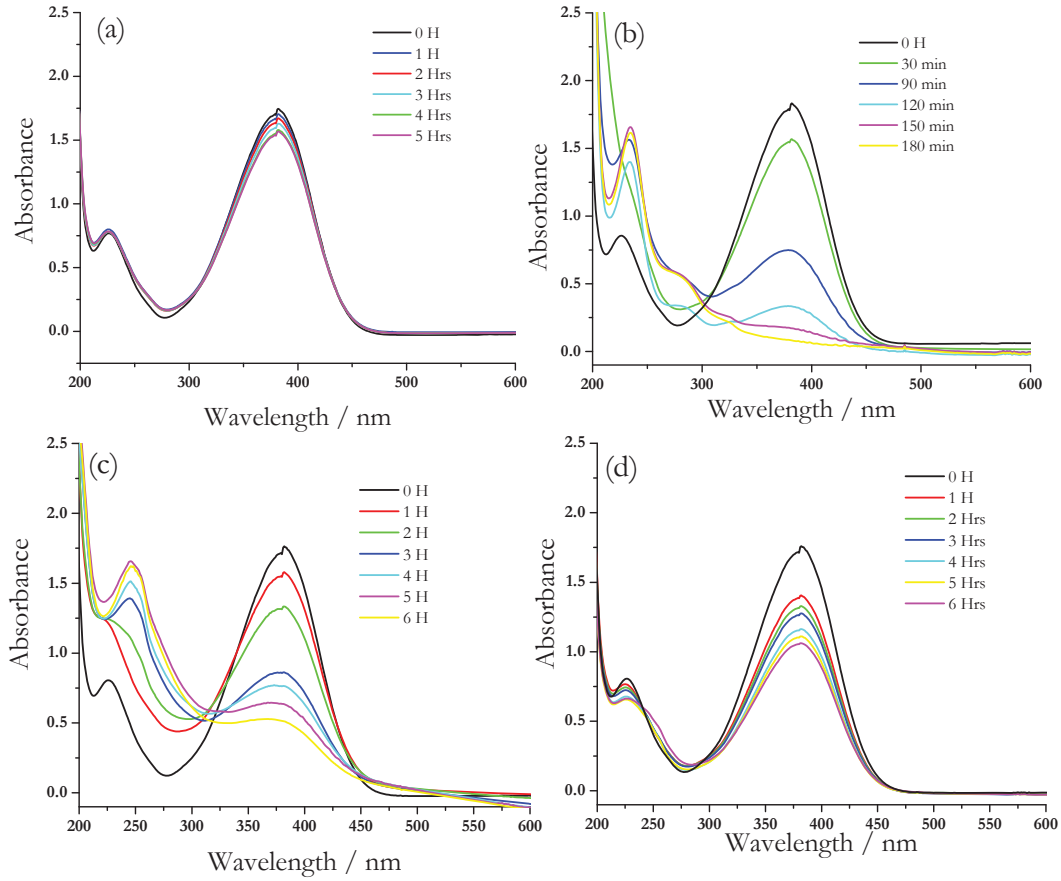

Figure 7. Relative concentration change of *p*-NA in the presence of Pt /($NaTaO_3$/MCM-48) composite catalysts. (a)p-NA without catalyst, (b) $NaTaO_3$ only, (c) $NaTaO_3$/MCM-48 (50-50), and (d) $NaTaO_3$/MCM-48 (10-90).

The plot of C/C_0 as a function of irradiation time, where C is *p*-NA concentration in reaction mixture and C_0 is the initial concentration of *p*-NA, is shown in Figure 8a. The relative concentration change of *p*-NA in the absence of a catalyst is approximately 10 % after 5 hours of irradiation. The concentration change in the presence of a composite catalyst ranges from 30 to 70%. The $NaTaO_3$/MCM-48 composites with 10-90 and 50-50 compositions gave the lowest and highest *p*-NA concentration change, respectively, after 5 hours of irradiation. As expected, relative concentration change increases with higher loading of $NaTaO_3$. If we just compare the data shown in Figure 8a as a function of total weight of catalyst (0.10 g) but not as a function of amount of $NaTaO_3$, pure $NaTaO_3$ causes the highest percent conversion in a given time. In order to correlate the weight of $NaTaO_3$ and the percent conversion and to evaluate photocatalytic efficiency, we calculated and compared the conversion by each composite catalyst as a function of composite weight and $NaTaO_3$ weight. This calculation is similar to turnover number (TON) and turnover frequency (TOF), but we used number of grams instead of number of active sites in the calculation. The turnover number is defined as the number of *p*-NA molecules converted into *p*-PDA per number of active sites of catalyst while TOF is defined as turnover number per second. The change in the concentration of *p*-NA after 3 hours of irradiation was used in the calculation. The amount of $NaTaO_3$ catalyst present in the SiO_2 matrix was analyzed by ICP spectrometer. Two samples with highest (50%) and lowest (10%) $NaTaO_3$ content were chosen for elemental analysis. The $NaTaO_3$:MCM-48 ratio obtained for the sample with 50%

nominal $NaTaO_3$ content was 46:54 while it was 8:92 for the sample with 10% $NaTaO_3$. A summary of conversions calculated as a function of composite weight and simple $NaTaO_3$ weight for different $NaTaO_3$/MCM-48 composite catalysts is tabulated in Table 2. The simple $NaTaO_3$ shows the highest conversion if the overall weight ($NaTaO_3$ + MCM) is used in the calculation. However, conversion numbers show a significant increase in composite catalysts when the calculations are based on just the $NaTaO_3$ content in the composite, not overall weight. In this case, it is clearly evident from the data that the conversion as a function of $NaTaO_3$ content increases with respect to decrease in $NaTaO_3$ content.

The reusability is a vital issue in applications of a photocatalyst. Therefore, reusability of composite photocatalysts was evaluated using the catalyst with 50% $NaTaO_3$ in $NaTaO_3$/MCM-48 composite under the same reaction conditions applied for photocatalytic activity testing. Based on relative concentration data acquired in 3 attempts for the same catalyst (Figure 8b), it is seen that the catalyst loses approximately 12 % of its initial activity after 3 consecutive attempts, calculated using data acquired after 5 hours of irradiation. SEM image of 50/50 MCM/NaTaO3 spent catalyst was acquired (Figure 9) in order to discern whether there is a significant change in morphology due to uv irradiation. It is evident that irradiation is not detrimental even though there is slight coagulation, which may cause drop in surface area. In fact this might be a reason why we see 12% activity reduction upon cycling.

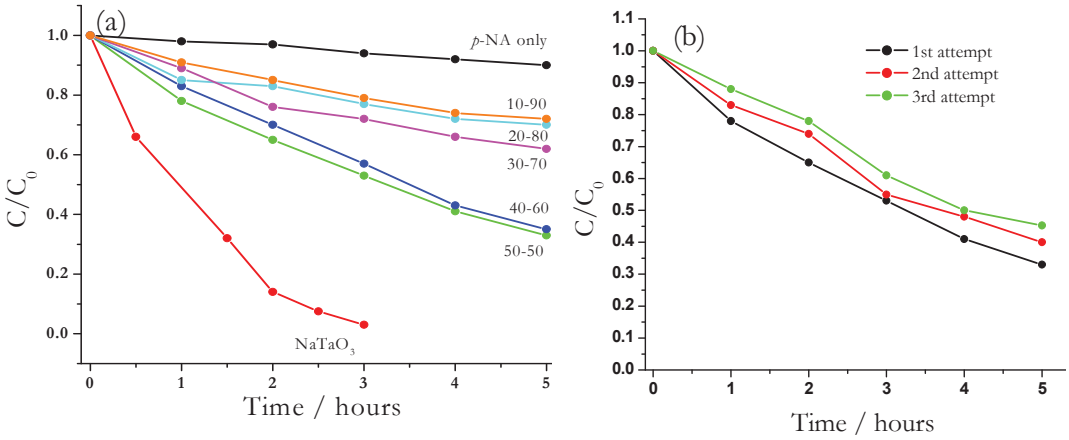

Figure 8. Plot of C/C_0 of composite photocatalysts as a function of time (a) and reproducibility of photocatalytic data for Pt /($NaTaO_3$/MCM-48) (b).

Table 2. Summary of conversion numbers of $NaTaO_3$/MCM-48 composite catalysts calculated from absorbance data at 3 hours of irradiation.

	Conversion per composite weight		Conversion per $NaTaO_3$ weight	
$NaTaO_3$:MCM	(molecules /g)	(molecules /g.s)	(molecules /g $_{NaTaO3}$)	(molecules/g $_{NaTaO3}$ .s
100 : 0	2.49×10^{19}	2.30×10^{15}	2.49×10^{19}	2.30×10^{15}
50 : 50	1.33×10^{19}	1.24×10^{15}	2.66×10^{19}	2.46×10^{15}
40 : 60	1.07×10^{19}	9.87×10^{14}	2.67×10^{19}	2.48×10^{15}
30 : 70	7.30×10^{18}	6.78×10^{14}	2.53×10^{19}	2.34×10^{15}
20 : 80	5.98×10^{18}	5.54×10^{14}	2.99×10^{19}	2.77×10^{15}
10 : 90	5.47×10^{18}	5.06×10^{14}	5.47×10^{19}	5.06×10^{15}

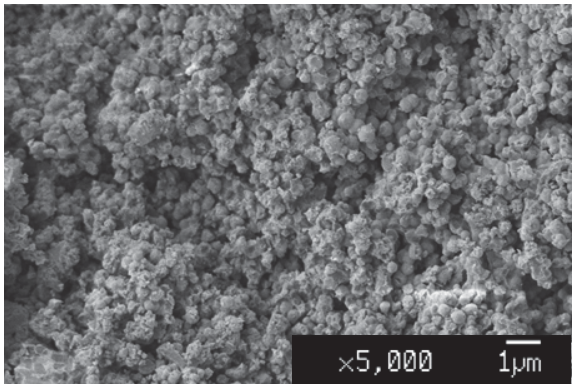

Figure 9. SEM image of 50/50 MCM/$NaTaO_3$ catalysts acquired after photocatalytic testing

Conclusions

Sol-gel method was used to synthesize a series of $NaTaO_3$/MCM-48 silica composite photocatalysts. Their physicochemical properties and photocatalytic activities in *p*-nitroaniline conversion into *p*-phenylenediamine were measured. The calculated conversion of *p*-nitroaniline by the composite photocatalysts is higher than that for pristine $NaTaO_3$ catalyst, which indicates a higher activity of conversion per gram of $NaTaO_3$ in composites. Nevertheless, it is difficult to find a clear correlation between the surface area and the activity even though the overall activity of composite catalysts is higher. Photocatalytic activity towards p-NA conversion is reproducible and the catalyst loses only 12 % of its activity after 3 consecutive attempts.

Acknowledgement

This work has been financially supported by the Wake Forest University Center for Energy, Environment, and Sustainability (CEES), and by the Triad Interuniversity Project (TIP) of Wake Forest University, North Carolina A & T University, University of North Carolina Greensboro, and Winston Salem State University.

References

[1] Kudo A and Miseki Y 2009 *Chem. Soc. Rev*. **38** 253-8
[2] Kudo A and Kato H 2000 *Phys. Lett*. **331** 373-7
[3] He Y, Zhu Y and Wu N 2004 *Solid State Chem*. **177** 3868-72
[4] T. Yokoi, T Sakuma K, Domen K, Tatsumi T and Kondo, K 2011 *Phys. Chem. Chem. Phys*. **13** 2563-70
[5] Osterloh F E 2008 *Chem. Mater* 20 35-54
[6] Parachino A, Laporte V, Sivula K, Grätzel M and Thimsen E, 2011 *Nat. Mater*. **10** 456-461
[7] Esswein A J, McMurdo M J, Ross P N, Bell A T and Tilley T D, 2009 *J. Phys. Chem. C* **113** 15068-72
[8] Rossmeisl J, Qu Z W, Zhu H, Kroes G J, J.K. Norskov, 2007 *J. Electroanal. Chem*. **607** 83-89
[9] Vazquez-zcuchillo O, Manzo-Robeldo A, Zanella Elizondo-Villareal R N and Cruz-Lopez A *Ultrason. Sonochem*. **20** 498-501
[10] Li X and Zang J 2011 *Catal. Commun*. **12** 1380-83
[11] Yi X, Li J, 2010 *J. Sol-Gel Sci. Technol*. **53** 480-484

[12] Lin W-H, Cheng C, Hu C-C and Teng H, 2006 *Appl. Phys. Lett*. **89** 211904-906
[13] Kato H and Kudo A,2001 *J. Phys. Chem B* **105** 4285-92
[14] Kato H, Kiyotaka K and Kudo A, 2003 *J. Am. Chem. Soc*. **125** 3082-89
[15] Mohamed R M and Aazam E S, 2014 *J. Ind. Eng. Chem*. **20** 4377-81
[16] Amano F, Nogami K, Tanaka M and Ohtani B, 2010 *Langmuir* **26** 7174-80
[17] Ryu S Y, Balcerski W, Lee T K and Hoffmann M R, 2007 *J. Phys. Chem. C* **111** 18195-203
[18] Zhang K, Yuan E-H, Xu L-L, Xue Q-S, Luo C, Albela B and Bonneviot L 2002 *Eur. J. Inorg. Chem*. **2012** 4183-89
[19] Peng R, Zhao D, Baltrusatis J, Wu C-M and Koodali R T 2012 *RSC Adv*. **2** 5754-67
[20] Aleksandrovic V and Djonlagic J 2001 *J. Serb. Chem. Soc*. **66** 139-152
[21] Peng R, Zhao D, Dimitrijevic N M, Rajh T and Koodali R T 2012 *J. Phys. Chem. C* **116** 1605-13
[22] Hu C-C and Teng H 2007 *Appl. Catal. A: General* **331** 44-50
[23] Tüysüz H and Chan C K 2013 *Nano Energy* **2** 116-123
[24] Senevirathne K, Burns A, Bussell M E and Brock S 2007 *Adv. Funct. Mater*. **17** 3933-39
[25] Ravikovitch P I, Vishnyakov A, Russo R and Neimark A V, 2000 *Langmuir* **16** 2311-20